https://doi.org/10.1016/j.jmmm.2018.08.018

Anomalous Hall effect in $Pt/Tb_3Fe_5O_{12}$ heterostructure: Effect of Compensation Point

Y. K. Liu, H.F. Wong, K.K. Lam, K.H. Chan, C.L. Mak and C.W. Leung[1]
Department of Applied Physics, The Hong Kong Polytechnic University, Hum Hom, Hong Kong, China

Abstract

Atomically-flat thin films of ferrimagnetic insulator $Tb_3Fe_5O_{12}$ (TbIG) were grown on (111)-orientated $Gd_3Ga_5O_{12}$ (GGG) substrates by pulsed laser deposition. Magnetic measurements indicated the easy magnetic axis of TbIG film was out-of-plane, as a result of the substrate-induced compressive in-plane strain of the film. The temperature dependence of anomalous Hall effect (AHE) in Pt/TbIG bilayer was systematically studied with the applied magnetic field normal to the film plane, with square hysteresis AHE loops being observed. Reversal of AHE sign occurred twice between 10 K and room temperature, one at 50 K and another around 220 K, the latter of which was accompanied by complex magnetization switching behavior. The peculiar behavior of AHE loop around 220 K is closely related to the compensation point of TbIG. On the other hand, the sign change at 50 K was attributed to the modification of Pt electronic structure by TbIG. Our results highlight the relation between the AHE of Pt and magnetic properties of TbIG, which can be used for probing the magnetism in TbIG.

* Electronic mail: dennis.leung@polyu.edu.hk

Introduction

Recent investigations on pure spin currents, which transport only spin angular moment but no net electrical charge flow, open new possibilities for both conducting and insulating spintronics systems [1-8]. In contrary to charge current, the spin current is not a conservative quantity. Up to now, pure spin current phenomena (such as spin Seebeck effect [4, 9], antiferromagnetic spin Seebeck effect [10], spin Hall effect [2, 7], inverse spin Hall effect [8, 11], spin pumping [12, 13], and magnetic nano-oscillator [1]) have been explored in various heterostructures consisting of normal metals (NM), antiferromagnetic metals (AFM), ferromagnetic metals (FM), and ferrimagnetic insulators (FI). In these heterostructures, high atomic-number metals such as Pt are used due to the strong spin-orbit coupling that results in larger spin Hall angles [12].

One type of widely studied heterostructures is the Pt/$Y_3Fe_5O_{12}$ bilayer [6, 14-19], where $Y_3Fe_5O_{12}$ (YIG) is an archetypal ferrimagnetic rare-earth insulator with the garnet structure ($Re_3Fe_5O_{12}$, ReIG) and possesses high Curie point (~550 K). In particular, a new type of magnetoresistance, called spin Hall magnetoresistance (SMR), has been found in Pt/YIG heterostructures [20], originating from the interplay between the spin accumulation at the NM/FI interface and the magnetization of the FI layer. In the SMR effect, charge current only passes through NM layer and cannot penetrate through the FI layer, but can generate spin accumulation near the NM/FI interface which is affected by the magnetization direction of FI layer.

On the other hand, anomalous Hall effect (AHE) in Pt layer has also been found in Pt/YIG heterostructure [14, 17, 21] similar to the Pt/normal FM [22]. The Hall response in FM contains the ordinary Hall effect (OHE) contribution (with a linear dependence on the applied magnetic field) and an AHE part (which is proportional

to the magnetization of FM and is closely related to the spin-orbital interaction). AHE loops observed in Pt/YIG system, however, are typically non-hysteresis [14, 17, 21]. Comparison with magnetic properties in YIG grown on gadolinium gallium garnet ($Gd_3Ga_5O_{12}$, GGG) substrate always exhibit in-plane magnetic anisotropy [14, 18, 23]. Furthermore, there is much controversy on whether the SMR and AHE observed in Pt/ReIG system is due to pure spin current or the magnetic proximity effect (MPE) [14, 16, 17, 21, 24, 25]. Therefore, it will be necessary to further study other Pt/ReIG heterostructures, in order to identify the role of ReIG in Pt/ReIG heterostructures.

In the present work, we investigate AHE behavior in a similar system of Pt on ferromagnetic insulator of terbium iron garnet $Tb_3Fe_5O_{12}$ (TbIG). The lattice of bulk TbIG is 12.436Å [26], which is much larger than that of YIG (12.376 Å) and GGG (12.383 Å). Thus an in-plane compressive strain is expected for TbIG films grown on GGG substrates, in contrary with that of YIG/GGG [15]. Another significant difference between TbIG and YIG is the presence of the compensation point (T_{comp} ~246 K) in TbIG [27], at which the net magnetic moment vanishes. As for the TbIG garnet, the magnetic moment of Tb^{3+} is antiparallel to the magnetic moment of Fe^{3+}, but at T_{comp} the Tb^{3+} magnetization will be equal to Fe^{3+} magnetization. Therefore, it will be of great interest to investigate the temperature dependence of AHE behavior in Pt/TbIG heterostructure, for obtaining further insight into the relation between the AHE of Pt and underlying FI.

Experiment

TbIG thin films were grown on (111)-orientated GGG substrates by pulsed laser deposition (PLD). A stoichiometric TbIG target was synthesized by the solid-state

reaction at 1400˚C. Focused KrF excimer laser pulses of wavelength λ = 248 nm were impinged to the TbIG target placed 5 cm away from the substrate. The laser energy and repetition rate were 1 J/cm^2 and 2 Hz, respectively. Films were grown at 710˚C in an oxygen ambient of 100 mTorr. Before deposition, the substrates were rinsed sequentially with acetone, ethanol and deionized water, and then annealed in oxygen at 1000˚C for 6 hours; these steps permit the reconstruction of the substrate surface and hence promotes the growth of smooth TbIG films. After deposition, the films were annealed *in situ* at 710˚C in an oxygen atmosphere of 10 Torr for 10 min. For the Hall measurements, 5 nm of Pt with Hall bar patterns (channel width: 160 μm, channel length: 500 μm) was deposited by rf sputtering through a stainless steel shadow mask, in a vacuum chamber of base pressure 1×10^{-7} Torr, using a target power of 60 W.

The microstructure of TbIG films were examined by high-resolution x-ray diffractometry (Smartlab, Rigaku, Japan) with 2θ scans and reciprocal space mapping (RSM). Surface morphology of TbIG films was characterized by atomic force microscopy (AFM, Asylum 3D infinity). Magnetic hysteresis loops were recorded by the standard vibrating sample magnetometer option of the physical property measurement system (PPMS, Quantum Design). Hall measurements were conducted in the PPMS with an applied current of 100 μA.

Results and Discussions

Fig. 1(a) displays the θ-2θ scan of the TbIG/GGG (111) film. The clear satellite fringes indicate a smooth film surface and sharp film/substrate interface. From this figure, one can extract the out-of-plane lattice spacing of d_{444} = 0.1842 nm for TbIG film, which is slight larger than the bulk value of 0.1795 nm. The rocking curve (inset of Fig.1(a)) gives a full-width at half-maximum (FWHM) of 0.07˚,

indicating a good epitaxial film quality. Given the lattice of GGG is 12.383Å, the TbIG film is imposed with an in-plane compressive stress. X-ray reciprocal space mapping (RSM) of the (444) reflection for the TbIG/GGG sample (Fig.1(b)) indicates a coherent growth, and the sharp peaks with clear fringes similar to that in Fig.1(a) further confirms the high quality of the TbIG film deposited. Surface topology of TbIG film (Fig.1(c)) indicates a root-mean-square roughness (σ_{rms}) value of 0.9Å, exhibiting a smooth surface.

Fig.1(d) shows the in-plane and out-of-plane magnetic hysteresis (*M*-*H*) loops of 30-nm thick TbIG film measured at room temperature. The out-of-plane hysteresis loop displays a much more squared shape compared to that of out-of-plane *M*-*H* loop, indicating an easy magnetization axis along the film normal plane. The perpendicular anisotropy of TbIG/GGG is attributed to the out-of-plane tensile stress and a positive magnetostriction constant [15]. This can be compared with YIG grown on (111) GGG substrates, which demonstrates a minute in-plane tensile stress and an in-plane anisotropy [28]. The accomplishment of out-of-plane easy axis in TbIG / (111) GGG is useful for studying the AHE in Pt/TbIG bilayer.

Temperature dependence of Hall measurements were performed in the PPMS system, and the schematic of the measurement is depicted in Fig.2(a). In all of the measurements, the magnetic field (*H*) was applied perpendicular to the current direction, and the rotation of *H* (denoted θ) was measured relative to the film normal direction. For checking the quality of the Pt film, Fig. 2(b) shows the temperature dependence of longitudinal resistance (R_{xx}), which decreases gradually with reducing temperature down to 20 K. A resistance minimum appears at around 17 K, which can be attributed to the weak localization of electrons similar to that observed in Pt/$Y_3Fe_5O_{12}$ bilayer [16]. The residual resistivity ratio, defined here as R_{xx}(300 K)/R_{xx}(10 K), is around 1.14, which is comparable with literature .

Fig.2(c) shows the θ dependence of Hall resistance (R_H) at 10 K. When H rotates from in-plane to out-of-plane, a hysteretic AHE behavior is observed in Pt/TbIG bilayer apart from the linear contribution of OHE; this is in contrast with the usual observations in YIG-based bilayer with nonhysteresis AHE behavior [14, 17, 29]. When the magnetic field is normal to film (θ = 0˚), one can extract the AHE resistance (R_{AHE}) by subtracting the linear OHE contribution (Fig.2(d)). The result indicates the TbIG/GGG sample shows an out-of-plane easy axis, thus the hysteresis AHE in Pt/TbIG/GGG enable electrical measurement of the magnetic state of the TbIG. In the following results, the OHE components are subtracted for more transparent analysis of the magnetic behavior.

To further investigate the AHE in Pt/TbIG bilayers, we depict the AHE loops (R_{AHE}-H) as a function of temperature with θ = 0˚ (Fig. 3), with the black arrows in the figure indicate the scanning field directions. All the AHE loops show hysteresis behavior, but one can notice that the *sign* of AHE is closely dependent on the temperature. We define R_{AHE}^0 as the R_{AHE} value at zero field when H scans from +9 T to 0 T. At low temperatures ($T \leq 40$ K), R_{AHE}^0 is positive with amplitude reducing from 2.8 mΩ (10 K, Fig. 2(d)) to 0.61 mΩ (40 K). However, when the temperature reaches 60 K, the *sign* of R_{AHE} is reverses (Fig. 3(b), R_{AHE}^0 = - 0.45 mΩ). With further increasing temperature up to 140 K, the magnitude of R_{AHE}^0 keeps rising up to 2.0 mΩ. At around 230 K, one finds yet another sign reversal of R_{AHE}^0 which lasts until room temperature, i.e. R_{AHE}^0 keeps the same positive sign and the amplitude of R_{AHE}^0 reduces with increasing temperature.

The complete temperature dependence profile of R_{AHE}^0 is shown in Fig. 4(a). As described before, at low temperatures (< 50 K) R_{AHE}^0 is positive and diminishes with rising temperature. A sign reversal occurs at 50 K before it reaches a

maximum amplitude at around 140 K. Beyond this point, the amplitude of R_{AHE}^{0} reduces with rising temperature again until 230 K, where R_{AHE}^{0} shows another sign reversal and retains positive up to room temperature. Peculiarities occurring around 50 K and 220 K, where the sign of R_{AHE}^{0} is switched, is the main topic of investigation in this work.

Apart from R_{AHE}^{0} magnitude, we also extracted the temperature dependence of coercive field (H_{C}) from the R_{AHE} curves (Fig. 4(b)); H_{C} is defined as the field at which the AHE resistance R_{AHE} becomes zero. Basically, H_{C} reduces with increasing temperature but shows an anomaly around 230 K. Comparison of R_{AHE}^{0} and H_{C} in Fig. 4 highlights the close link between R_{AHE}^{0} sign transition and the H_{C} anomaly. Note that in the figure we plot the H_C at 50 K separately: as R_{AHE}^{0} vanishes at this temperature, no clear hysteretic behaivour could be detected, and we isolate this specific data from the main H_C-T trace.

In ReIG, both Fe^{3+} and rare earth (Re) ions (Tb^{3+} for TbIG) make contribution to the net moment, but the spins of rare earth ions are antiferromagnetically coupling with that of Fe^{3+}[27, 30]. At some intermediate temperatures, the net magnetic moment of garnet is zero when Re ion moments cancel with that of Fe^{3+} ions, which is the origin of the compensation point [27]. For bulk TbIG T_{comp} = 246 K [27]; in the present work T_{comp} as in Hall measurement of Pt/TbIG heterostructure is near 220 K, which can be resulted from the strain effect or oxygen vacancy in the TbIG thin film [31].

To probe the AHE behavior near T_{comp}, Fig. 5 shows the AHE loops of Pt/TbIG heterostructure between 215 K and 225 K. Interestingly, in these temperatures, the loops show three distinct loops (denoted I, II and III); this is different from R_{AHE}-H loops measured at other temperatures (Fig. 3) or in Pt/YIG system [16, 17, 29] in

which a simple hysteresis loop is observed. Increasing the temperature from 215 K to 225 K, loops II and III shift to zero field, and at 225 K loop I almost disappeared. At 230 K, Pt/TbIG bilayer shows only one hysteresis loop again with high coercive field (Fig. 3e).

Such a peculiar behavior can be closely related to the complex magnetic structure of TbIG near T_{comp}. TbIG and related ReIG with heavy Re ions (such as $Gd_3Fe_5O_{12}$, GdIG) with cubic structures belong to the space group *Ia*3*d* [32, 33]. The Tb^{3+} ions are located at the 24 dodecahedral sites (*c*) with magnetization M_{Tb}, while Fe^{3+} ions in the tetrahedral (*d*) and octahedral (*a*) sites give a resultant moment M_{Fe} which is antiparallel to M_{Tb} [26, 30, 32]. At T_{comp}, M_{Tb} is equal to M_{Fe} and as a result the total magnetic moment of TbIG vanishes [34]. Theoretical calculations of GdIG using molecular-field analysis indicated that near the compensation point, it is possible to have multiple sublattice moment configurations upon increasing magnetic field at constant temperatures [35]. As for the TbIG, its magnetic structure is expected to be similar with GdIG, which contains three magnetic sublattices [35]. Three distinct loops in Fig.5 should therefore represent the magnetic moment switching of these sublattices. According to Ref. [35], at temperatures near the compensation point, the sublattice reorientation takes place with increasing magnetic fields. This is consistent with the demonstration of multiple AHE loops (I, II and III) near T_{comp} (Fig. 5), and the observations can be attributed to the complex magnetic structures and coupling between Fe^{3+} and Tb^{3+} ions.

Anomalous temperature dependence of R_{AHE}-H curves also occurs around 50 K. Fig. 6 shows the variation of R_{AHE}-H curves between 45 and 55 K. One can notice the sign flipping of R_{AHE}^0 at the two temperature ends. Such sign changes of AHE at low temperature has been observed in Pt/YIG based systems [14, 17, 21] and in

other ferromagnetic materials [36, 37]. Taking ferromagnetic metal $SrRuO_3$ as an example, the R_{AHE} sign change with temperature has been attributed to the singularity in the band structure [37]. Recently, it was found that AHE in Pt film can be induced and the sign change temperature can also be tuned by ionic liquid gating [21], which was explained in the terms of local moments induced by electrical field. In the Pt/YIG bilayer, the proximity of the Pt to the YIG leads to the band splitting of the Pt 5*d* band and the lowering of the density of states at the Pt Fermi level [16]. First-principles relativistic band calculations for Pt indicate that the intrinsic spin Hall effect can be found due to the resonant contribution from the spin-orbit splitting of the doubly-degenerated *d* band at high-symmetry *L* and *X* points near the Fermi level [38]. Therefore, spin splitting and electrical structure of Pt film will be affected by the exchange interaction within adjacent ferromagnetic insulator [6, 18, 19].

For ReIG films grown on GGG substrates, the colossal paramagnetic contribution from the substrates makes it difficult to discern the intrinsic magnetic moment of the films [39]. To this end, we thinned down the (111) GGG substrate and measured the hysteresis loop of the TbIG film by vibrating sample magnetometry (VSM). Temperature dependences of the coercive field (H_C^M) (Fig. 7(a)) and saturation moment M_s (Fig. 7(b)) were extracted from the magnetic measurement. Except the regions near T_{comp} where meaningful results could not be extracted due to the vanishing magnetic moment [27], we acquired square *M*-*H* loops after subtracting the paramagnetic substrate contribution from the original data. Comparing Fig. 7(a) to Fig. 4(b), one can find that H_C^M decreases with nearly identical temperature dependence as H_C measured by AHE, namely a drop of H_C^M with increasing *T* until 140 K and then raises with further increasing *T*, and finally decreases from around T_{comp} to room temperature. The temperature dependent of

M_s of our TbIG film is the same as that observed in TbIG bulk [27], where M_s decreases with rising temperature up to T_{comp} before it re-emerges again above T_{comp}. The exception deviation between Fig. 4(b) and Fig. 7 is at 50 K, where a sudden drop in H_C^M was not observed, which is due to the different nature of measurements used. The difference of H_C in AHE (Fig. 4(b)) and H_C^M in VMS measurement at 50 K is attributed to the inability to yield AHE signals at that temperature [14, 17, 21], which requires further investigation.

Conclusion

In summary, we deposited high-quality TbIG films on GGG(111) substrates, which exhibited an out-of-plane magnetic anisotropy. Magnetotransport measurements of Pt/TbIG bilayer demonstrated square hysteretic AHE loops at room temperature. Systematically investigating the temperature dependence of AHE loops of Pt/TbIG heterostructure indicated abnormal Hall resistance sign change at 50 K and 220 K. In the latter temperature, which coincides with the compensation point of TbIG such that the magnetic moment of TbIG vanishes, complex AHE behavior was recorded and the coercive field reaches the maximum.

Acknowledgments

This work was supported by the National Natural Science Foundation of China (Grant No. 51502129), the Hong Kong Research Grant Council (PolyU 153027/17P) and The Hong Kong Polytechnic University (1-ZVGH).

Figure captions:

Figure 1. Structural and magnetic properties of TbIG film. (a) X-ray diffraction 2θ-θ scan of TbIG film grown on (111)-oriented GGG substrate. Inset: rocking curve of (444) reflections around TbIG film. (b) X-ray reciprocal space mapping around the (444) peak of TbIG film and GGG substrate. The vertical dashed line represents the in-plane lattice parameter of TbIG and GGG substrate. (c) AFM topographic image of TbIG film. (d) In-plane and out-of-plane normalized magnetic hysteresis loops of TbIG film at room temperature.

Figure 2. Hall measurements on a Pt/TbIG bilayer device. (a) Hall device schematics, coordinate systems and the electrical measurement set-up. (b) Temperature-dependent Pt thin film resistance grown on TbIG/GGG substrates. (c) Hall resistance R_H measured with sweeping magnetic field at θ=0˚, 45˚, 90˚, 135˚, 180˚. (d) R_{AHE}-H loop after subtracting the linear, ordinary Hall contribution. Black arrows indicate the sweeping field directions. In all these Hall measurements, the magnetic field was always normal to the current. All measurements were performed at 10 K.

Figure 3. Temperature dependent R_{AHE}-H loops of Pt/TbIG. R_{AHE} as a function of the out-of-plane magnetic field for different temperatures of 40K (a), 60K (b), 140K (c), 210K (d), 230K (e), 300K (f). The black arrows indicate the sweeping magnetic field directions.

Figure 4. Determination of magnetic properties of Pt/TbIG bilayer from Hall measurements. (a) R_{AHE}^0 (blue) an $|R_{AHE}^0|$ (red) as a function of temperature. (b) Temperature dependence of coercive field H_C obtained from the R_{AHE}-H loops. The star indicates the data at 50 K.

Figure 5. R_{AHE}-H loops around T_{comp} of TbIG. R_{AHE}-H loops measured at 215K (a), 220K (b), 225K (c). Obviously, more than one jump reversals can be observed around 220K. The blue lines and arrows indicate data recorded during a +H→-H sweep and red lines and arrows indicate data recorded during a -H→+H sweep.

Figure 6. Details of Hall sign change in R_{AHE}-H loops of TbIG around 50K. R_{AHE}-H loops measured at 45K (a), 50K (b), 55K (c). The signs of R_{AHE} are different for above and below 50 K. The black arrows indicate the sweeping field directions.

Figure 7. Coercivity (a) and saturation moment (b) of TbIG film as a function of temperature, as measured by VSM. The H_C^M and M_s of TbIG films were obtained by VSM measurements from films grown on a 0.1 mm-thickness (111) GGG substrate.

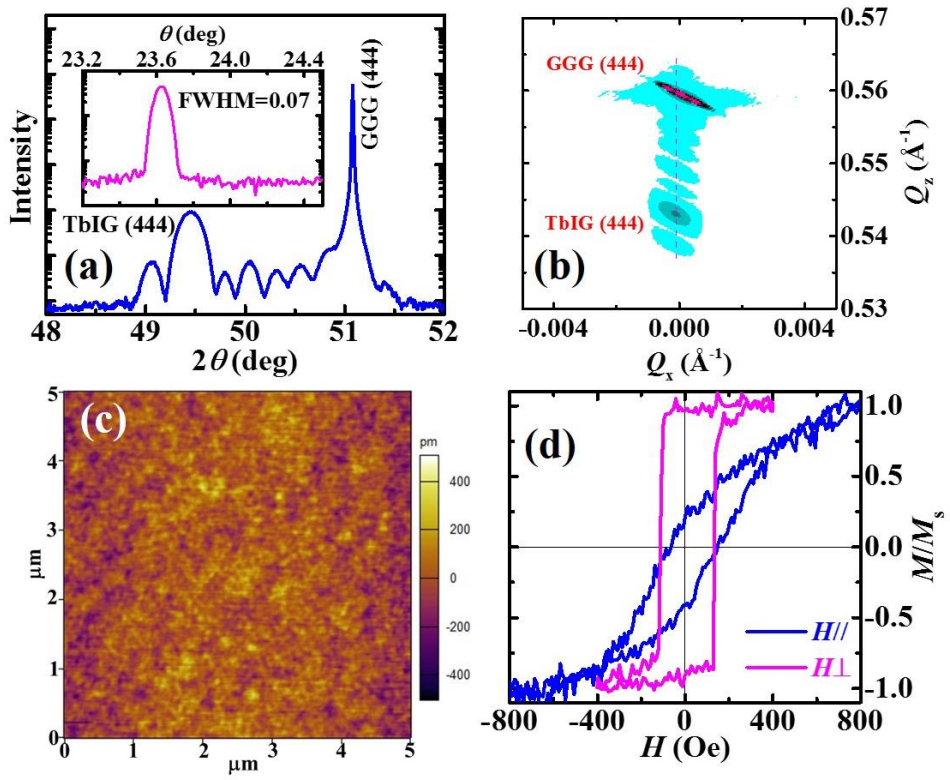

Figure 1.

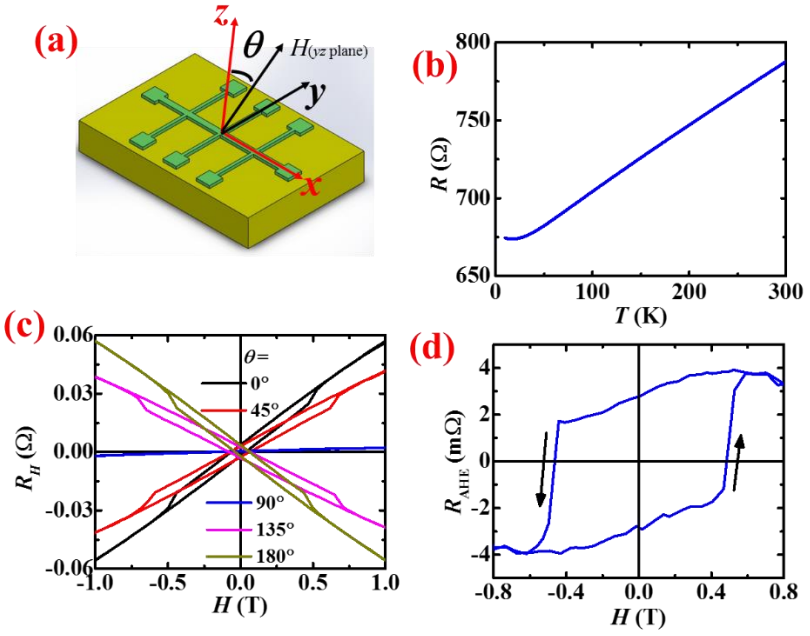

Figure 2.

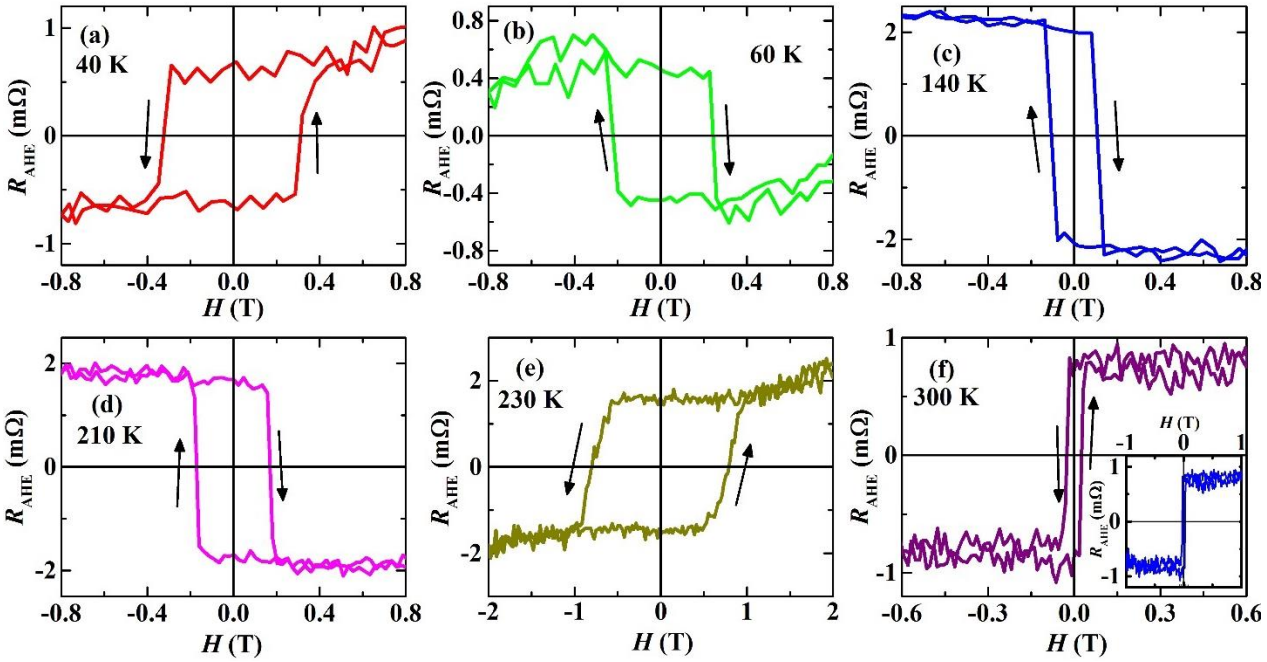

Figure 3.

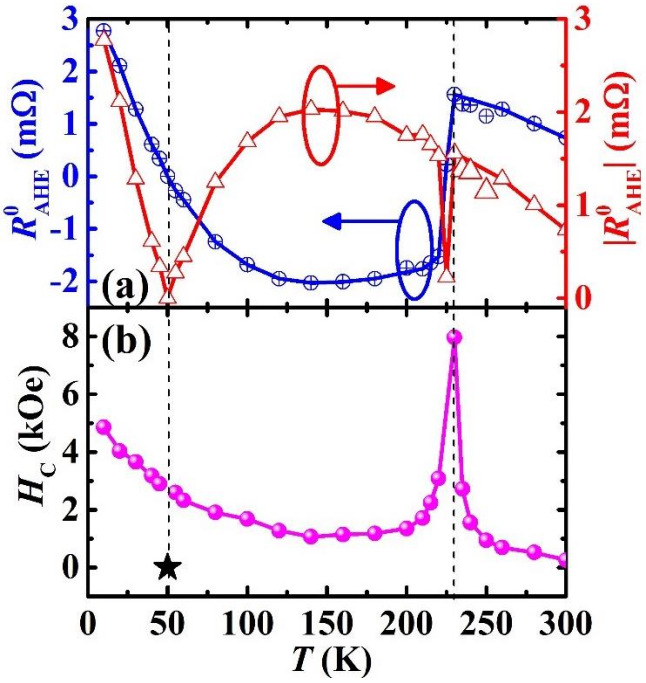
(a)
(b)
R^0_{AHE} (mΩ)
$|R^0_{AHE}|$ (mΩ)
H_C (kOe)
T (K)
3
2
1
0
-1
-2
8
6
4
2
0
0
50
100
150
200
250
300

Figure 4.

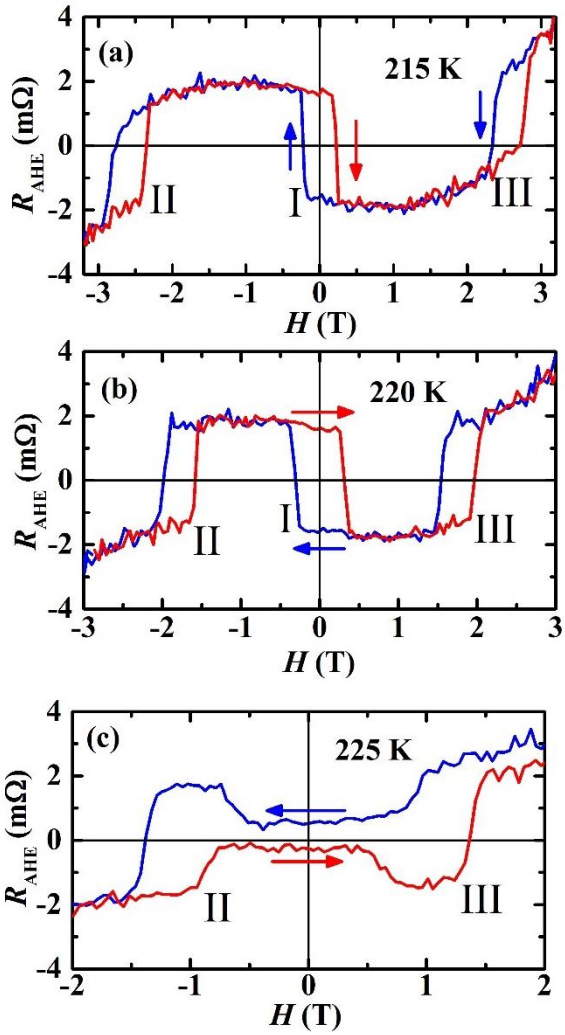
(a)
215 K
II
I
III
R_{AHE} (mΩ)
H (T)
(b)
220 K
II
I
III
R_{AHE} (mΩ)
H (T)
(c)
225 K
II
III
R_{AHE} (mΩ)
H (T)

Figure 5.

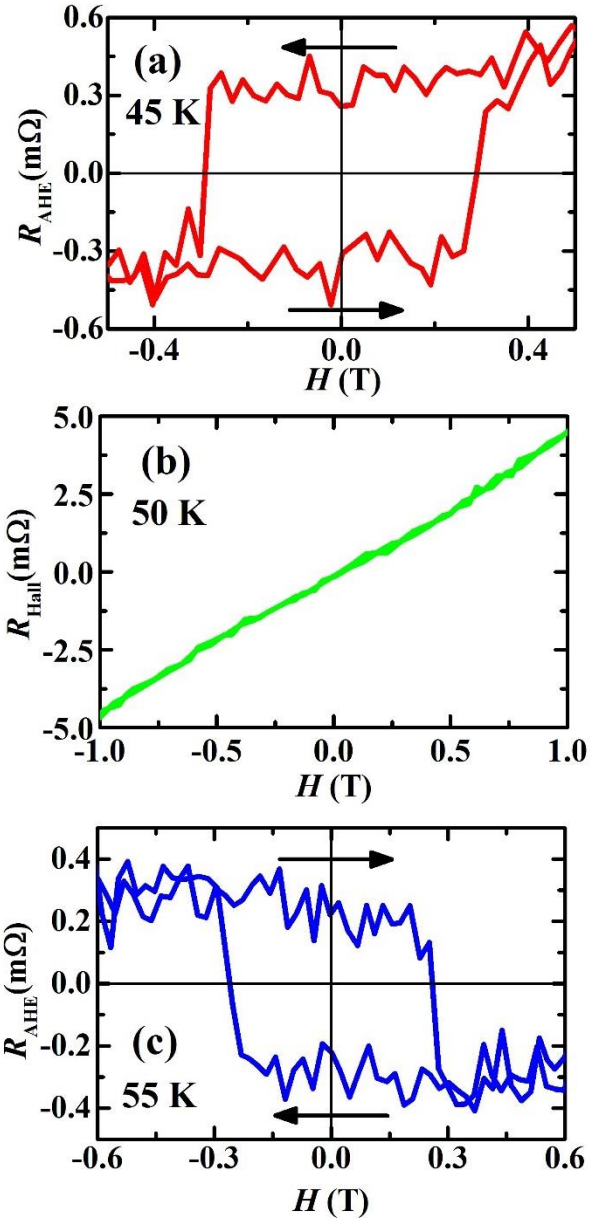
(a)
45 K
R_{AHE} (mΩ)
0.6
0.3
0.0
-0.3
-0.6
-0.4
0.0
0.4
H (T)
(b)
50 K
R_{Hall} (mΩ)
5.0
2.5
0.0
-2.5
-5.0
-1.0
-0.5
0.0
0.5
1.0
H (T)
(c)
55 K
R_{AHE} (mΩ)
0.4
0.2
0.0
-0.2
-0.4
-0.6
-0.3
0.0
0.3
0.6
H (T)

Figure 6.

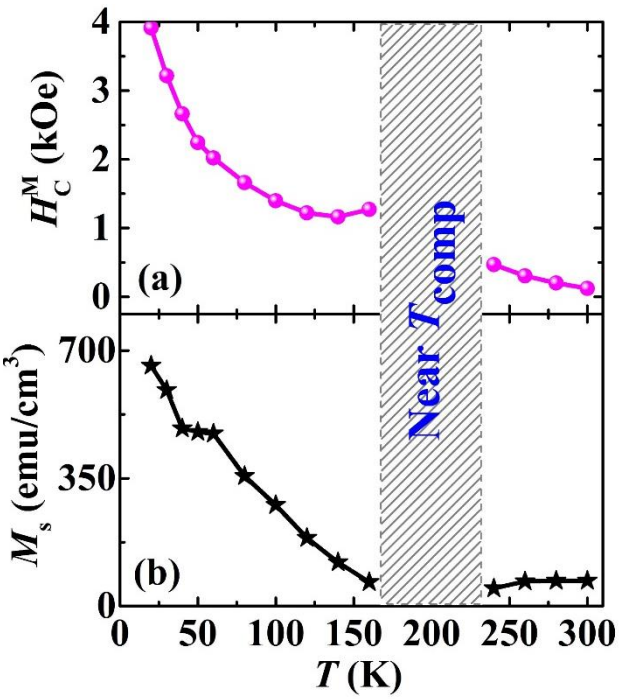
4
3
2
1
0
H_C^M (kOe)
(a)
Near T_{comp}
700
350
0
M_s (emu/cm^3)
(b)
0
50
100
150
200
250
300
T (K)

Figure 7.

References

[1] V.E. Demidov, S. Urazhdin, H. Ulrichs, V. Tiberkevich, A. Slavin, D. Baither, G. Schmitz, S. Demokritov, Magnetic nano-oscillator driven by pure spin current, Nat. Mater., 11 (2012) 1028 - 1031.

[2] L. Liu, C.-F. Pai, Y. Li, H.W. Tseng, D.C. Ralph, R.A. Buhrman, Spin-Torque Switching with the Giant Spin Hall Effect of Tantalum, Science, 336 (2012) 555-558.

[3] A. Slachter, F.L. Bakker, J.-P. Adam, B.J.v. Wees, Thermally driven spin injection from a ferromagnet into a non-magnetic metal, Nat. Phys., 6 (2010) 879-882.

[4] K. Uchida, S. Takahashi, K. Harii, J. Ieda, W. Koshibae, K. Ando, S. Maekawa, E. Saitoh, Observation of the spin Seebeck effect, Nature, 455 (2008) 778-781.

[5] T. Yang, T. Kimura, Y. Otani, Giant spin-accumulation signal and pure spin-current-induced reversible magnetization switching, Nat. Phys., 4 (2008) 851-854.

[6] A. Kirihara, K.-i. Uchida, Y. Kajiwara, M. Ishida, Y. Nakamura, T. Manako, E. Saitoh, S. Yorozu, Spin-current-driven thermoelectric coating, Nat. Mater., 11 (2012) 686-689.

[7] N.P. Stern, S. Ghosh, G. Xiang, M. Zhu, N. Samarth, D.D. Awschalom, Current-induced polarization and the spin Hall effect at room temperature, Phys. Rev. Lett., 97 (2006) 126603.

[8] J.C. Rojas-Sanchez, N. Reyren, P. Laczkowski, W. Savero, J.P. Attane, C. Deranlot, M. Jamet, J.M. George, L. Vila, H. Jaffres, Spin pumping and inverse spin Hall effect in platinum: the essential role of spin-memory loss at metallic interfaces, Phys. Rev. Lett., 112 (2014) 106602.

[9] T. Seki, Y. Hasegawa, S. Mitani, S. Takahashi, H. Imamura, S. Maekawa, J. Nitta, K. Takanashi, Giant spin Hall effect in perpendicularly spin-polarized FePt/Au devices, Nat. Mater., 7 (2008) 125-129.

[10] S.M. Wu, W. Zhang, A. Kc, P. Borisov, J.E. Pearson, J.S. Jiang, D. Lederman, A. Hoffmann, A. Bhattacharya, Antiferromagnetic Spin Seebeck Effect, Phys. Rev. Lett., 116 (2016) 097204.

[11] K. Ando, E. Saitoh, Observation of the inverse spin Hall effect in silicon, Nat. Commun., 3 (2012) 629.

[12] O. Mosendz, J.E. Pearson, F.Y. Fradin, G.E. Bauer, S.D. Bader, A. Hoffmann, Quantifying spin Hall angles from spin pumping: experiments and theory, Phys. Rev. Lett., 104 (2010) 046601.

[13] M.V. Costache, M. Sladkov, S.M. Watts, C.H. van der Wal, B.J. van Wees, Electrical detection of spin pumping due to the precessing magnetization of a single ferromagnet, Phys. Rev. Lett., 97 (2006) 216603.

[14] S.Y. Huang, X. Fan, D. Qu, Y.P. Chen, W.G. Wang, J. Wu, T.Y. Chen, J.Q. Xiao, C.L. Chien, Transport magnetic proximity effects in platinum, Phys. Rev. Lett., 109 (2012) 107204.

[15] M. Kubota, A. Tsukazaki, F. Kagawa, K. Shibuya, Y. Tokunaga, M. Kawasaki, Y. Tokura, Stress-Induced Perpendicular Magnetization in Epitaxial Iron Garnet Thin Films, Appl. Phys. Exp., 5 (2012) 103002.

[16] Y.M. Lu, Y. Choi, C.M. Ortega, X.M. Cheng, J.W. Cai, S.Y. Huang, L. Sun, C.L. Chien, Pt magnetic polarization on Y3Fe5O12 and magnetotransport characteristics, Phys. Rev. Lett., 110 (2013) 147207.

[17] B.F. Miao, S.Y. Huang, D. Qu, C.L. Chien, Physical origins of the new magnetoresistance in Pt/YIG, Phys. Rev. Lett., 112 (2014) 236601.

[18] V. Castel, N. Vlietstra, B.J. van Wees, J.B. Youssef, Frequency and power dependence of spin-current emission by spin pumping in a thin-film YIG/Pt system, Phys. Rev. B, 86 (2012).

[19] W. Lin, C.L. Chien, Electrical Detection of Spin Backflow from an Antiferromagnetic Insulator/Y_{3}Fe_{5}O_{12} Interface, Phys. Rev. Lett., 118 (2017) 067202.

[20] H. Nakayama, M. Althammer, Y.T. Chen, K. Uchida, Y. Kajiwara, D. Kikuchi, T. Ohtani, S. Geprags, M. Opel, S. Takahashi, R. Gross, G.E. Bauer, S.T. Goennenwein, E. Saitoh, Spin Hall magnetoresistance induced by a nonequilibrium proximity effect, Phys. Rev. Lett., 110 (2013) 206601.

[21] S. Shimizu, K.S. Takahashi, T. Hatano, M. Kawasaki, Y. Tokura, Y. Iwasa, Electrically tunable anomalous Hall effect in Pt thin films, Phys. Rev. Lett., 111 (2013) 216803.

[22] N. Nagaosa, J. Sinova, S. Onoda, A.H. MacDonald, N.P. Ong, Anomalous Hall effect, Rev. Mod. Phys., 82 (2010) 1539-1592.
[23] C. Tang, M. Aldosary, Z. Jiang, H. Chang, B. Madon, K. Chan, M. Wu, J.E. Garay, J. Shi, Exquisite growth control and magnetic properties of yttrium iron garnet thin films, Appl. Phys. Lett., 108 (2016) 102403.
[24] M. Althammer, S. Meyer, H. Nakayama, M. Schreier, S. Altmannshofer, M. Weiler, H. Huebl, S. Geprägs, M. Opel, R. Gross, D. Meier, C. Klewe, T. Kuschel, J.-M. Schmalhorst, G. Reiss, L. Shen, A. Gupta, Y.-T. Chen, G.E.W. Bauer, E. Saitoh, S.T.B. Goennenwein, Quantitative study of the spin Hall magnetoresistance in ferromagnetic insulator/normal metal hybrids, Phys. Rev. B, 87 (2013).
[25] J. Li, Y. Xu, M. Aldosary, C. Tang, Z. Lin, S. Zhang, R. Lake, J. Shi, Observation of magnon-mediated current drag in Pt/yttrium iron garnet/Pt(Ta) trilayers, Nat. Commun., 7 (2016) 10858.
[26] H. Fuess, G. Bassi, M. Bonnet, A. Delapalme, Neutrom scattering of terbium strsucture refinement and magnetic moments, Solid State Commun., 18 (1976) 557-562.
[27] S. Geller, J.P. Remeika, R.C. Sherwood, H.J. Williams, G.P. Espinosa, Magnetic Study of the Heavier Rare-Earth Iron Garnets, Phys. Rev., 137 (1965) A1034-A1038.
[28] A. Mitra, O. Cespedes, Q. Ramasse, M. Ali, S. Marmion, M. Ward, R.M.D. Brydson, C.J. Kinane, J.F.K. Cooper, S. Langridge, B.J. Hickey, Interfacial Origin of the Magnetisation Suppression of Thin Film Yttrium Iron Garnet, Sci. Rep., 7 (2017) 11774.
[29] T. Lin, C. Tang, J. Shi, Induced magneto-transport properties at palladium/yttrium iron garnet interface, Appl. Phys. Lett., 103 (2013) 132407.
[30] S. Geschwind, L.R. Walker, Exchange Resonances in Gadolinium Iron Garnet near the Magnetic Compensation Temperature, J. Appl. Phys., 30 (1959) S163-S170.
[31] J. Cramer, E.J. Guo, S. Geprags, A. Kehlberger, Y.P. Ivanov, K. Ganzhorn, F. Della Coletta, M. Althammer, H. Huebl, R. Gross, J. Kosel, M. Klaui, S.T.B. Goennenwein, Magnon Mode Selective Spin Transport in Compensated Ferrimagnets, Nano Lett., 17 (2017) 3334-3340.
[32] S. Geller, M.A. Gilleo, The crystal structure and ferrimagnetism of yttrium-iron garnet, $Y_3Fe_2(FeO_4)_3$, J. Phys. Chem. Solids, 3 (1957) 30-36.
[33] F. Sayetat, Huge Magnetostriction in $Tb_3Fe_5O_{12}$, $Dy_3Fe_5O_{12}$, $Ho_3Fe_5O_{12}$, $Er_3Fe_5O_{12}$ garnets, Journal of Magnetic and Magnetic Materials, 58 (1986) 334-336.
[34] P. Hansen, P. Röschmann, W. Tolksdorf, Saturation magnetization of gallium-substituted yttrium iron garnet, J. Appl. Phys., 45 (1974) 2728-2732.
[35] J. Bernasconi, D. Kuse, Canted Spin Phase in Gadolinium Iron Garnet, Phys. Rev. B, 3 (1971) 811-815.
[36] W.J. Xu, B. Zhang, Z.X. Liu, Z. Wang, W. Li, Z.B. Wu, R.H. Yu, X.X. Zhang, Anomalous Hall effect in Fe/Gd bilayers, Europhys. Lett., 90 (2010) 27004.
[37] Z. Fang, N. Nagaosa, K.S. Takahashi, A. Asamitsu, R. Mathieu, T. Ogasawara, H. Yamada, M. Kawasaki, Y. Tokura, K. Terakura, The Anomalous Hall Effect and Magnetic Monopoles in Momentum Space, Science, 302 (2003) 92-95.
[38] G.Y. Guo, S. Murakami, T.W. Chen, N. Nagaosa, Intrinsic spin Hall effect in platinum: first-principles calculations, Phys. Rev. Lett., 100 (2008) 096401.
[39] C.O. Avci, A. Quindeau, C.F. Pai, M. Mann, L. Caretta, A.S. Tang, M.C. Onbasli, C.A. Ross, G.S. Beach, Current-induced switching in a magnetic insulator, Nat. Mater., 16 (2017) 309-314.